


Article

Design and Implementation of a Robotic Hip Exoskeleton for Gait Rehabilitation

Shi-Heng Hsu¹, Chuan Changcheng¹, Heng-Ju Lee²  and Chun-Ta Chen^{1,*}

¹ Department of Mechatronic Engineering, National Taiwan Normal University, 162, Section 1, He-Ping East Road, Taipei 106, Taiwan; louis94777471@gmail.com (S.-H.H.); s920365@gmail.com (C.C.)

² Department of Physical Education and Sport Sciences, National Taiwan Normal University, 162, Section 1, He-Ping East Road, Taipei 106, Taiwan; hjlee@ntnu.edu.tw

* Correspondence: chenct@ntnu.edu.tw; Tel.: +886-277-493-528; Fax: +886-223-583-074

Abstract: In this paper, a four degrees-of-freedom robotic hip exoskeleton was proposed for gait rehabilitation. The robotic hip exoskeleton was designed with active flexion/extension and passive abduction/adduction at each hip joint to comply with the movement of the thigh. Due to each user's different lower limbs characteristics and unknown torques at hip joints, model-free linear extended state observer (LESO)-based controllers were proposed for rehabilitation gait control. The prototypes of the robotic hip exoskeleton and controller designs were validated and compared through walking and ascending rehabilitation experiments. Additionally, a motion captured system and EMG signals were used to investigate the walking assistance of the robotic hip exoskeleton.

Keywords: robotic hip exoskeleton; gait; rehabilitation; LESO; FTSMC



Citation: Hsu, S.-H.; Changcheng, C.; Lee, H.-J.; Chen, C.-T. Design and Implementation of a Robotic Hip Exoskeleton for Gait Rehabilitation. *Actuators* **2021**, *10*, 212. <https://doi.org/10.3390/act10090212>

Academic Editor: André Preumont

Received: 26 July 2021

Accepted: 26 August 2021

Published: 29 August 2021

Publisher's Note: MDPI stays neutral with regard to jurisdictional claims in published maps and institutional affiliations.



Copyright: © 2021 by the authors. Licensee MDPI, Basel, Switzerland. This article is an open access article distributed under the terms and conditions of the Creative Commons Attribution (CC BY) license (<https://creativecommons.org/licenses/by/4.0/>).

1. Introduction

Accidents, aging, stroke, and neural diseases cause the impairment of motor functions. Those with movement difficulties have their daily living activities hindered. Especially, the lower limb dysfunctions always cause unnatural gait patterns and thus reduce mobility. Therefore, a rehabilitation exercise should be executed to help those impaired to recover motor abilities [1]. However, the conventional therapist-led manual assisting rehabilitation treatment is a repetitive, progressive, and typically time consuming and labor-intensive task.

Currently, research studies on robots demonstrate that robotic devices can assure consistency in repetitive rehabilitation therapy and are available for rehabilitation treatment [2]. Among them, wearable robotic exoskeletons are characterized by light weight, portability, low cost, and safety and thus receive attention for facilitating rehabilitation training or power assistance [3,4].

Wearable robotic exoskeletons are a mechanical structure whose joints and links have compatibility with the limbs of human beings [5]. In applications to assist lower extremities, many robotic lower-limb exoskeletons, such as BLEEX [6], AUTONOMYO [7], PH-EXOS [8], HUMA [9], and HAL [10], have been devised to implement rehabilitation or augment power. Generally, these robotic exoskeletons are classified as hip–knee–ankle motion, hip–knee motion, hip motion, or knee motion based on the various assistance functions [11]. Although the movements of the human lower limbs mainly involve rotation about the hip joints, knee joints, and ankle joints, studies have shown that the human hip joint provides 45% of the mechanical power during a gait cycle, and the hip joint actuation plays the most important role in walking [12]. As a consequence, a robotic hip exoskeleton can be utilized enough to strengthen the wearers' hip joint mobility and assist users with walking impediments. Assisted rehabilitation with a robotic hip exoskeleton is promising to improve gait function.

As a user wears a robotic hip exoskeleton to execute a gait rehabilitation exercise, the robotic hip exoskeleton must convey forces to actuate the lower limbs to track the planned

rehabilitation trajectory slowly, smoothly, and safely [13]. The mechanical design and control technologies of a robotic exoskeleton must play a critical role in the rehabilitation effects. For the mechanical design, Lee et al. [14] developed a robotic hip exoskeleton with two active DOFs and two passive DOFs for rehabilitation and gait improvement. The experiments showed that the robotic hip exoskeleton can improve the user's gait function and muscle effort, reducing the metabolic cost of walking. Giovacchini et al. [15] proposed four DOFs of active pelvis orthosis for motion assistance. The series elastic actuators (SEAs) were introduced into the robotic exoskeleton for low output impedance and energy storage. The experimental results demonstrated that the exoskeleton could provide smooth assistive torque for the hip joints.

In control technologies for robotic hip exoskeletons, different approaches to the generation of assistive torque or rehabilitation trajectories were proposed. In [15], Giovacchini et al. also presented a hierarchical architecture control system for the robotic hip exoskeleton, in which a high-level controller was used for the generation of torque references and a low-level PID controller for the regulation of desired torque. Nagarajan et al. [16] proposed an integral admittance shaping algorithm to control robotic hip exoskeleton, such that the desired dynamic response of the human–exoskeleton system was achieved. An adaptive admittance controller taking into account the interaction between the user and the robotic hip exoskeleton was proposed by Zhang et al. [17] to assist walking and maintain walking stability. The results showed that the exoskeleton could provide adaptive assistance torque for the user as needed. Wu et al. [18] developed a robotic hip exoskeleton to assist locomotion for those with walking impairments. The flexion/extension of the six-DOF hip exoskeleton was actuated through Bowden cable transmission. A cascaded PID controller for the passive control of the hip exoskeleton was used to perform trajectory tracking, and a fuzzy adaptive controller for the active control was applied to perform walking assistance. The conducted experiments presented the effectiveness of walking assistance and reduction of muscular power consumption.

From the aforementioned observations of mechanical design, most robotic hip exoskeletons were developed with two DOFs for each hip joint, one for the active flexion/extension movement and the other for the passive abduction/adduction movement, but very few, with the exception of [8], considered internal/external rotation. Moreover, for the above control designs, model-based controllers needing a dynamic model were always used for rehabilitation control or power assistance of robotic hip exoskeletons. However, the dynamic formulation of exoskeletons is always arduous. It is also time-consuming in computation if a model-based controller is implemented into the rehabilitation exercise. Moreover, due to uncertainties from the exoskeleton or a user's unpredicted applied forces, torque sensors or EMG sensors in the referred references were used to regulate the adaptive assistance torque or generate a torque reference as needed to provide the walking assistance. However, the appended sensors make the control complex, and also the cost increases.

In this paper, inspired by human anatomy, a robotic hip exoskeleton was developed for walking rehabilitation, in which two DOFs in the hip joint were considered to allow for easy use by the wearers. Instead of additional sensors for joint torque, such as torque sensors or EMG sensors [18], a linear extended state observer (LESO) was designed to estimate a wearer's applied torques and human/exoskeleton uncertainties. Furthermore, the LESO-based fast terminal sliding mode controller (FTSMC) without the detailed exoskeleton model was proposed to track the planned trajectories during the walking training. Extending our previous conference paper [19] in which only the preliminary results based on the LADRC were presented, in the current paper, except for the proposed LESO-based FTSMC for gait rehabilitation control, the associated stability proof was presented. More concrete experimental tests and evaluations were also conducted to investigate the effects of the robotic hip exoskeleton on gait rehabilitation, e.g., rehabilitation experiments on walking, gait rehabilitation while suffering instant spasm and tremor, rehabilitation experiments on ascending, walking experiments for different subjects, and evaluation of rehabilitation assistance. A discussion and conclusions are given in detail in Sections 6 and 7, respectively.

2. Design and Building of Robotic Hip Exoskeleton

A user wears a robotic hip exoskeleton to improve the mobility of hip joints while executing gait rehabilitation or to reduce the metabolic consumption while powering the lower limbs for coming to assistance; the robotic hip exoskeleton should be as light-weight as possible. Moreover, the exoskeleton should be better able to comply with the movement of lower limbs in an anatomical structure. Inspired by the movement of the human's lower limbs, the design aims to develop a kinematically-compatible robotic hip exoskeleton to assist walking for rehabilitation.

2.1. Robotic Hip Exoskeleton Building

In general, there are three rotational degrees-of-freedom at each hip joint. Mainly, a human's walking is dominated by the flexion/extension motion. Abduction/adduction is related to control of walking balance and turning. Thus, the proposed robotic hip exoskeleton for gait rehabilitation is displayed in Figure 1a, in which the thigh link of the hip joint mechanism is mounted to the U frame and is rotated to generate the flexion/extension motion by a MAXON DC brushless motor (EC 60 flat) with a current driver (ESCON50/8). A 1:24 planet reducer is connected to the motor. The passive abduction/adduction rotation at the hip joint allows for the lateral motion of legs. The U frame is made of aluminum alloy, and its two ends are each connected to a strap. Inside the U frame, foam is attached for improvement of comfort. The exoskeleton can thus be put on by mounting the U frame to a wearer's waist and then fastening the two waist straps together.

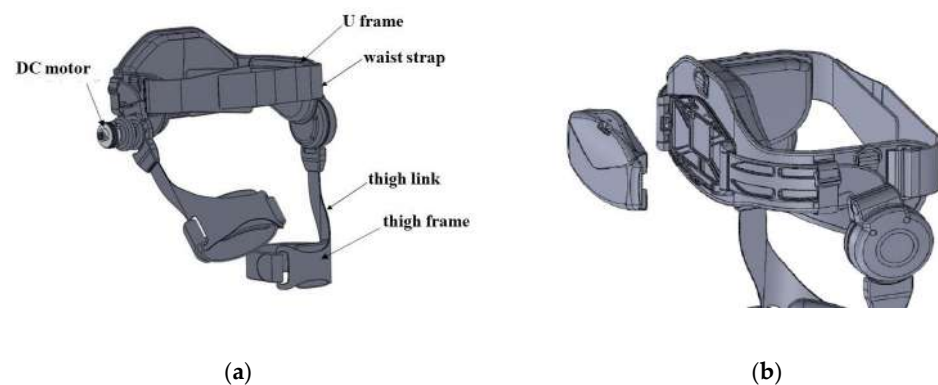


Figure 1. (a) Proposed robotic hip exoskeleton design, and (b) back pack for integration of electric devices.

Each aluminum alloy formed thigh link is made with a thigh frame and can be fixed to the thighs also using straps, such that power can be transferred to the lower limbs to assist walking or the sit-to-stand movement. Moreover, a stopper is installed in the U frame to limit an overshoot of rotation to protect users due to a possible wrong operation. The NI-mRio is for a controller, and drivers and batteries are integrated into the back pack for easy carrying, as shown in Figure 1b. This PLA plastic back pack was built using a 3D printer. Each joint is mounted with a high-resolution incremental encoder (Encoder MILE) with a resolution of 2048 counts per turn for measurement of joint angles. As shown in Figure 2, this robotic hip exoskeleton allows the flexion/extension rotation from -70° to 75° . The designed low-cost and lightweight robotic hip exoskeleton weighs 2.4 kg, and it can be used to assist walking for patients suffering from lower limb muscle dysfunction.

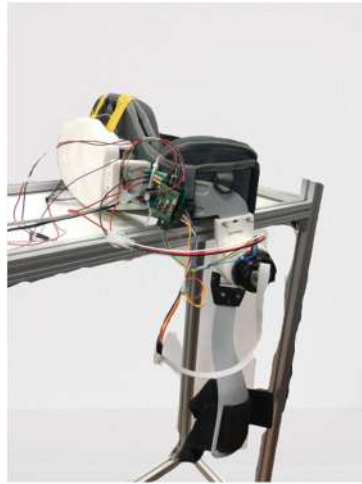


Figure 2. Robotic hip exoskeleton system building.

2.2. Electronics Design

The required actuation unit, angle sensors, and main control board are integrated to the robotic hip exoskeleton as presented in Figure 3. A NI MyRIO is embedded to control the robotic hip exoskeleton system. The MyRIO system consists of two kinds of modules, including reconfigurable IO modules (RIO) and FPGA modules, a real-time controller, and an Ethernet expansion chassis. The NI 9234 and NI 9263 modules that are installed in the cRIO 9072 enable analog-to-digital (AD) and digital-to-analog (DA) conversions. The input signals of the four channels of the NI 9234 are buffered, conditioned, and sampled by a 24-bit Delta-Sigma ADC. The analog outputs are enabled by NI 9263 through four channels with the specification of ± 10 V, 16-bit, 100 kS/s. Two serial lithium batteries with a total of 26 V supply all the required powers for actuators, sensors, and the controller. The control algorithms and measurements were developed mainly in the Labview system.

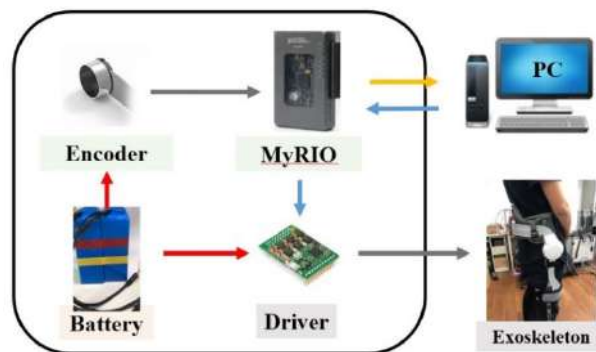


Figure 3. Control circuit and peripherals.

While operating the robotic hip exoskeleton system, the hip joint angle is read into the computer through the MyRIO. The computer calculates and synthesizes control commands to the exoskeleton. The controller for the actuators outputs a control signal to a channel as per our developed gait rehabilitation control algorithms. The system driver converts the control signal to enable the robotic hip exoskeleton to apply the corresponding actuating torques to drive a planned walking event.

3. Walking Dynamics and LESO-Based Controller Design

A complete walking period contains the stance phase of single leg/double legs and the swing phase. At the stance phase, a human being applies torque at the hip joints to maintain the posture stability, and the hip joint angles will not vary so largely. At the swing phase, torque is exerted by a human being to lift the lower limb, and then the leg is put

down to make the heel touch the ground. Therefore, the walking dynamics are distinct for these two phases.

3.1. Walking Dynamics

A user executes walking rehabilitation with a robotic hip exoskeleton, and the parameters of the wearer's lower limbs and the exoskeleton are coupled into the walking dynamics such that the lower limb can be simplified as a link with an attached equivalent end point mass. At the swing phase, the walking dynamics can be formulated by the oscillated model of single link; while at the stance phase, an inverted simple pendulum model is used for the dynamics. As a result, the unified walking dynamics for the swing and stance can be formulated as

$$M\ddot{\theta} + G = \tau_r + \tau_h, \quad (1)$$

in which θ is the hip joint angle; the inertia term M includes the mass and the moment of inertia of a lower limb as well as of the thigh link of the exoskeleton; the gravitational term G is the function of the mass of the lower limb and the thigh link. Additionally, M and G are configuration-dependent, τ_r is the output torque from the robotic hip exoskeleton for power assistance or gait rehabilitation, and τ_h is the exerted hip joint torque of the human being.

While implementing the gait rehabilitation, the robotic hip exoskeleton is given a rehabilitation trajectory to allow the wearer's thigh to follow the planned gait trajectory. However, the wearers' inertias are not exactly known and are different for individuals. As such, a model-based controller is not available without any compensation. Moreover, the exerted hip joint torque depends on gaits and the muscle strength of a lower limb, and each wearer has a different hip joint torque τ_h during walking. Currently, it is not easy to measure the human's hip joint torques using a torque sensor. As a result, a wearer's applied hip joint torque, τ_h , is unknown for the robotic hip exoskeleton and generally is regarded as an external disturbance. In this regard, in the paper, a disturbance observer, LESO, was proposed to estimate these uncertainties and the hip joint torques, and then the LESO-based controllers will be developed for gait rehabilitation control.

3.2. LESO Design

The advantage of LESO may estimate the dynamic uncertainties and exerted torques without a detailed system model. This effective approach extends another state to approximate the total system uncertainties and external disturbances in real time [20].

By inversion of the inertia term, also defining $\tau_r = u$ and introducing a user-defined control gain b_0 , Equation (1) can be expressed as

$$\ddot{\theta} = f + b_0 u, \quad (2)$$

in which $f = M^{-1}(\tau_h - G\theta) + bu - b_0 u$ accounts for the combined effects of internal dynamics and external disturbances on angular acceleration.

Rewriting Equation (2) in a state space, and also augmenting another state by defining $x_1 = \theta$, $\dot{x}_1 = x_2$, $\dot{x}_2 = x_3 + b_0 u$, $\dot{x}_3 = \dot{f}$, the dynamic equations are expressed in a compact form as

$$\begin{cases} \dot{x} = Ax + Bu + Eh \\ y = Cx \end{cases}, \quad (3)$$

in which $A = \begin{bmatrix} 0 & 1 & 0 \\ 0 & 0 & 1 \\ 0 & 0 & 0 \end{bmatrix}$, $B = [0 \quad b_0 \quad 0]^T$, $C = [1 \quad 0 \quad 0]$, $E = [0 \quad 0 \quad 1]^T$,

$h = \dot{f}$ being the part of jerk and physically bounded, and $x_3 = f$ being the added augmented state.

According to the state space expression for the dynamic Equation (3), the state observer predicting an estimate of the state of (3) can be designed as [21]

$$\begin{cases} \dot{z} = Az + Bu + L(y - \hat{y}) \\ \hat{y} = Cz \end{cases}, \quad (4)$$

in which $z = [z_1 \ z_2 \ z_3]^T$, being the estimation of the system state $x = [x_1 \ x_2 \ x_3]^T$, is the state vector of the observer, $L = [\beta_1 \ \beta_2 \ \beta_3]^T$ is the observer gain vector, and \hat{y} is the estimate of the system output y .

In Equation (4), z_3 is the estimation of f . Moreover, the tracking errors of the observer are defined as $e = x - z$; the error dynamics are then derived by Equations (3) and (4) as

$$\dot{e} = (A - LC)e + Eh = A_e e + d, \quad (5)$$

$$\text{in which } A_e = A - LC = \begin{bmatrix} -\beta_1 & 1 & 0 \\ -\beta_2 & 0 & 1 \\ -\beta_3 & 0 & 0 \end{bmatrix}.$$

3.3. LESO-Based PD Controller Design

As the active disturbance rejection control (ADRC) concept suggests [22], if the total disturbance is estimated and then used to try to eliminate the unknown total disturbance, the tracking errors of a system can be compensated by a PD type of controller.

Let \hat{f} be the estimate of f , and the control input u of the robotic hip exoskeleton be specified as

$$u = (-\hat{f} + u_0)/b_0, \quad (6)$$

Substituting Equation (6) into Equation (2), the dynamics are reduced to

$$\ddot{\theta} = (f - \hat{f}) + u_0 \approx u_0. \quad (7)$$

From Equation (7), the closed-loop dynamics can be made easily controllable by ADRC that tries to eliminate the estimated errors on f . Finally, the new control input u_0 can be synthesized in a PD type of control as

$$u_0 = k_p(\theta_d - z_1) + k_d(\dot{\theta}_d - z_2), \quad (8)$$

in which $\theta_d, \dot{\theta}_d$ are the predefined hip joint angles and joint rates.

Combining LESO and ADRC, the LADRC is composed, or the so-called LESO-based PD controller whose control structure is presented in Figure 4. Moreover, the control gains k_p, k_d can be specified as $k_d = 2\omega_c, k_p = \omega_c^2$ according to the separation principle of eigenvalues, in which ω_c is the user-defined frequency bandwidth [23].

3.4. LESO-Based SMC Design

In LADRC, the linear feedback control is synthesized by the estimated system state instead of the measured joint angles of the robotic hip exoskeleton. Sliding mode control (SMC) has the characteristics of simple control and easy implementation and has been successfully applied to many nonlinear systems. Moreover, SMC is an effective technique relative to the parametric uncertainties and external disturbances. The desired closed-loop performance of SMC is first defined by a sliding surface that the SMC specifies. Here the time-varying sliding surface is defined as

$$s = ce + \dot{e}, \quad (9)$$

in which $e = \theta_d - \theta$ is the hip joint angle errors with respect to the planned hip joint trajectory. The positive constant c is related to the desired performance of the closed-loop system.

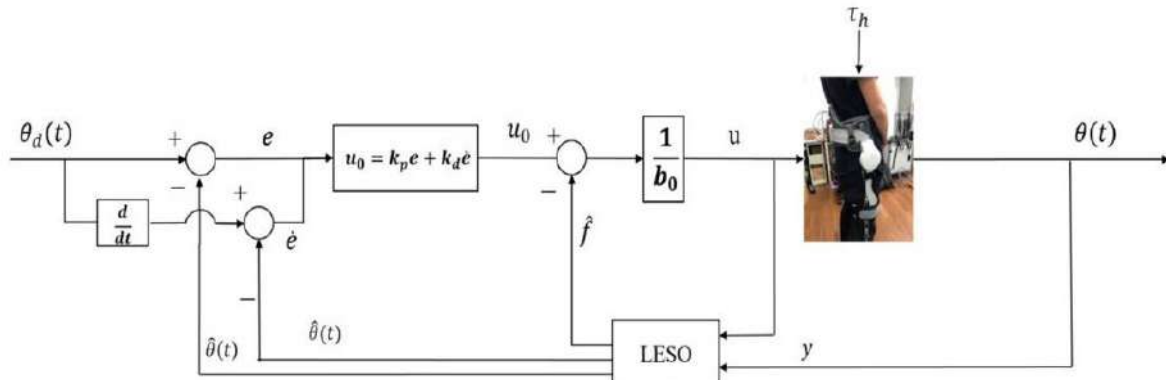


Figure 4. Control structure of LADRC.

A sliding mode controller comprises the nominal control u_{eq} that is determined by making the derivative of the sliding surface zero and the reaching control u_r for the system disturbances. At the reaching phase, the designed hitting control law compels the system trajectories onto the sliding surface. If the system state slides to the origin along a trajectory in a sliding mode, it remains on the sliding surface. As such, trajectory tracking is completed. The reaching control u_r is expressed traditionally in a sign function that always excites a chattering and results in damage. Instead, a hyper-tangent function is proposed for the reaching control to account for the uncertainties and eliminate the chattering. In total, the control input takes the form

$$u(t) = u_{eq}(t) + u_r(t) = (\ddot{\theta}_d - \hat{f} + c\dot{e})/b_0 + (\alpha \tanh(s) + \epsilon s)/b_0, \tag{10}$$

in which coefficients α, ϵ are positive, and can be defined by the following stability analysis.

A Lyapunov candidate $V(t)$ is chosen as

$$V = \frac{1}{2}s^2. \tag{11}$$

The stability is analyzed by differentiating (11) as

$$\dot{V} = s\dot{s} = s(-f + \hat{f} - \alpha \tanh(s) - \epsilon s) = s\Delta f - \alpha s(\tanh(s)) - \epsilon s^2 \leq |s||\Delta f| - \alpha |s||\tanh(s)| - \epsilon |s|^2 = |s|(|\Delta f| - \alpha |\tanh(s)| - \epsilon |s|), \tag{12}$$

in which $\Delta f = -f + \hat{f}$ is the observed disturbance error.

To stay on the sliding mode surface during the dynamic variation, the parameters α and ϵ must be chosen to let $\dot{V} < 0$ for $e \neq 0$. Moreover, as time approaches infinity, from Equation (5), with A_e being Hurwitz, $|\Delta f|$ is bounded, and the system is thus guaranteed stable [24].

The control structure of the LESO-based SMC that combines LESO and SMC is shown in Figure 5. In performing rehabilitation training, the planned hip joint angles θ_d are designated as the rehabilitation trajectories. The control signals u for the robotic hip exoskeleton are synthesized by the LESO-based SMC, actuating the DC motor to produce torques to drive the exoskeleton.

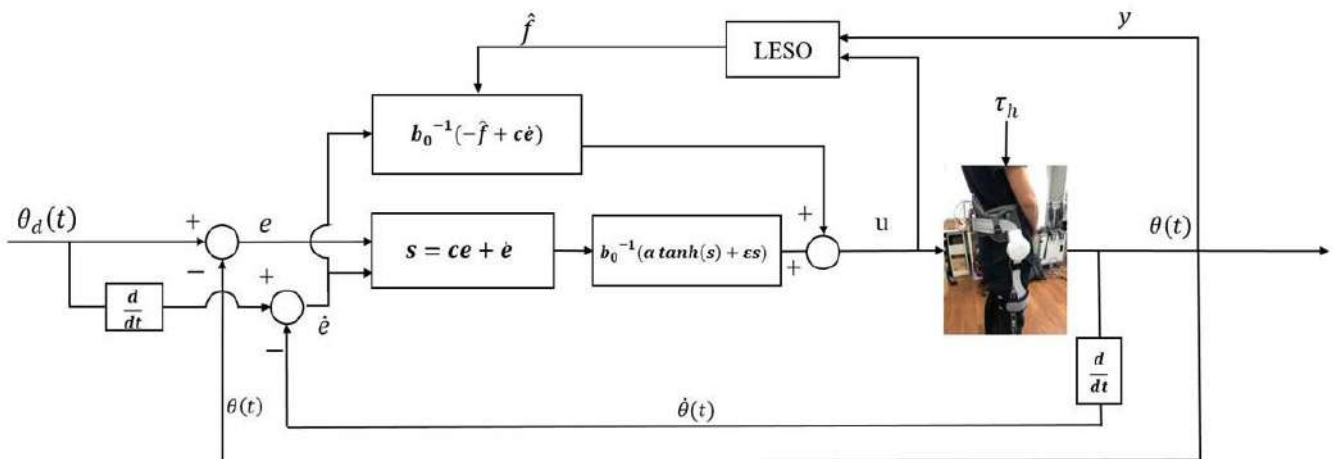


Figure 5. Control structure of LESO-based SMC.

3.5. LESO-Based FTSMC Design

To further improve the performance, a LESO-based fast terminal slide mode controller (FTSMC) is presented to control the robotic hip exoskeleton. In comparison with the SMC, the FTSMC can approach a designed sliding surface rapidly so that a system can be stabilized at a finite time.

In FTSMC, a sliding surface is defined as

$$s = \alpha e + \dot{e} + \beta e^{q/p}, \tag{13}$$

in which α, β, p, q are positive. Additionally, p, q are odd and coprime with $p > q$.

As the tracking error $e \gg 0$, the αe term in the sliding surface s has the faster approaching law, but as the error $e \rightarrow 0$, this term $\beta e^{q/p}$ will dominate the approaching law and make the system converge to a stable state rapidly [25].

The total control for the LESO-based FTSMC is designed as

$$u(t) = u_{eq}(t) + u_r(t) = (-\hat{f} + \alpha \dot{e} + \beta e^{(q-p)/p} \dot{e}) + (\varnothing s + r s^{n/m}), \tag{14}$$

in which the parameters \varnothing, r, n, m are positive, and n, m are odd and coprime each other.

The parameters $\alpha, \beta, \varnothing, r$ can be chosen based on the stability analysis following the above procedure for the LESO-based SMC, such that the derivative of a Lyapunov function $\dot{V} \leq 0$. The control structure for the LESO-based FTSMC is shown in Figure 6.

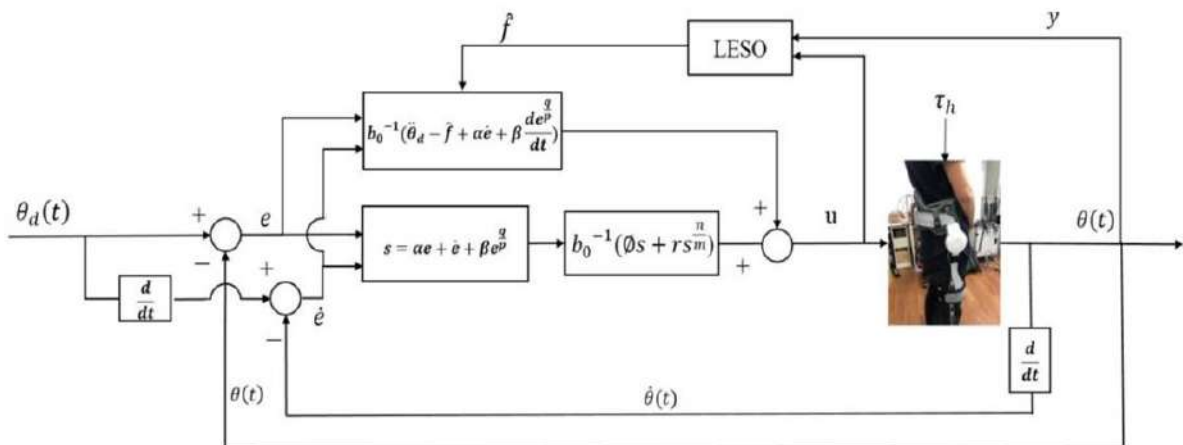


Figure 6. Control structure of LESO-based FTSMC.

4. Implementation of Walking Rehabilitation

The effects of the proposed robotic hip exoskeleton on gait rehabilitation were investigated. As shown in Figure 7, a healthy subject A with 1.72 m height/68 kg weight wore the robotic hip exoskeleton to execute rehabilitation exercises. For now, only the right leg was actuated and tested. The predefined trajectories of the hip joint were specified by the measurement of the joint angles according to the normal gaits. The trajectory tracking experiments were then conducted to implement the gait rehabilitation motions. The required parameters for the proposed controllers were as follows: in the LADRC, $k_p = 100$, $k_d = 20$, $\omega_0 = 100$; in the LESO-based SMC, $c = 50$, $\alpha = 50$, $\varepsilon = 50$; in the LESO-based FTSMC, $\alpha = 1$, $\beta = 1$, $p = 21$, $q = 19$, $\varnothing = 1$, $r = 1$, $m = 3$, $n = 1$. For all controllers, $b_0 = 10$.

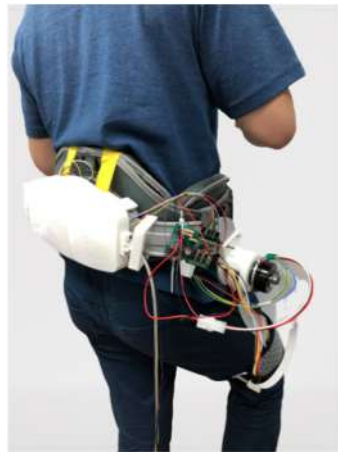


Figure 7. A subject wearing the robotic hip exoskeleton.

4.1. Walking Rehabilitation Experiment

As shown in Figure 8, the walking experiments for gait rehabilitation were conducted with two walking speeds: 0.15 m/s and 0.225 m/s. The hip joint trajectories were planned in advance. Three controllers, LADRC, LESO-based SMC, and LESO-based FTSMC, were employed and compared in terms of tracking performance.



Figure 8. Walking experiments for gait rehabilitation with robotic hip exoskeleton.

Figures 9 and 10 present the trajectories of the hip joint for the three controllers at the two different walking speeds. It was seen that the LADRC on the rehabilitation trajectory tracking had the worst performance because of the effects of a linear controller for the nonlinear system. LESO-based FTSMC apparently had superior tracking performance.

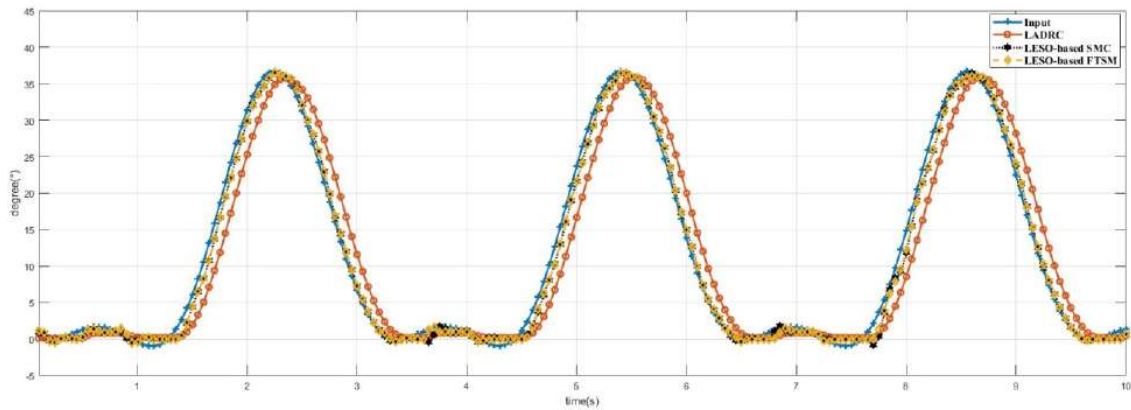


Figure 9. Trajectories of hip joint at walking speed = 0.15 m/s.

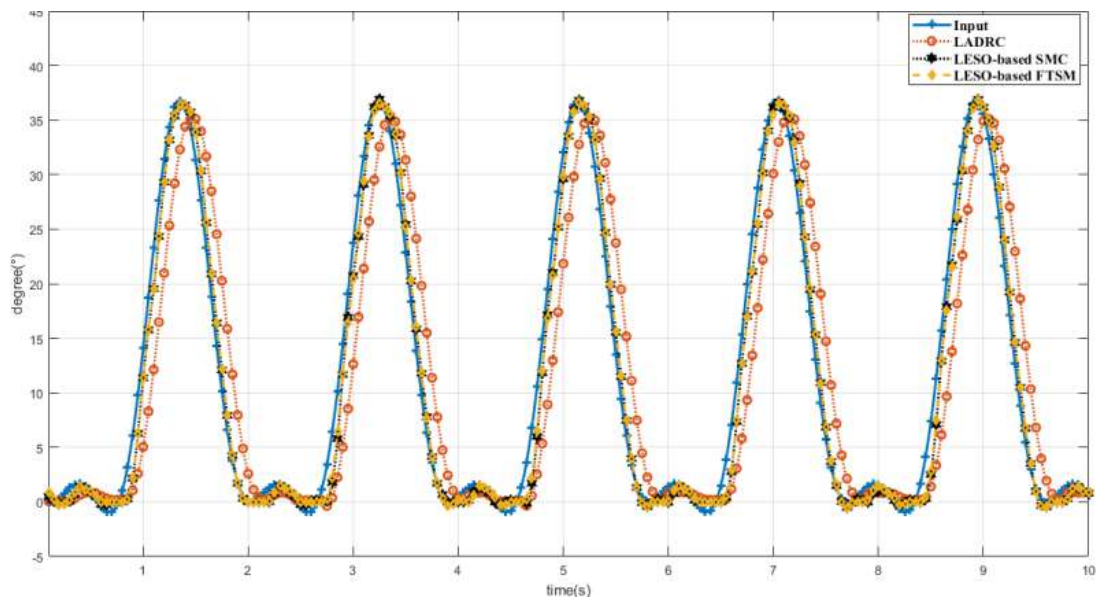


Figure 10. Trajectories of hip joint at walking speed = 0.225 m/s.

The RMS errors for the three controllers at the two walking speeds are shown in Table 1, in which $RMSE = \sqrt{\frac{\sum_{j=1}^n (\theta_j - \theta_{jd})^2}{n}}$, and θ_j is the measured hip joint angle, and θ_{jd} is the planned hip joint angle. It was demonstrated that the RMSEs were statistically and significantly lowered using the LESO-based FTSMC, and a better tracking performance for the robotic hip exoskeleton was achieved. Moreover, as the walking speed increased, LADRC presented a larger tracking error. However, for the other controllers, the tracking errors only increased slightly.

Table 1. RMSE of hip joint trajectories for LADRC, LESO-based SMC, LESO-based FTSMC.

Controller	Walking Speed	
	0.225 m/s	0.15 m/s
LADRC	6.008533°	3.685461°
LESO-based SMC	1.858353°	1.172696°
LESO-based FTSMC	1.821815°	1.145927°

4.2. Gait Rehabilitation while Suffering from Instant Spasm and Tremor

During the gait rehabilitation process, spasm and tremor may occur and affect the ensuing rehabilitation procedure [26]. If the phenomena are detected and possibly cause an unsafe situation for the user, the exercising process may have to be halted.

Sometimes with some manifestations, for instance, the cogwheel phenomenon, spasm, clonus or fasciculations, tremors may occur during a rehabilitation process. These phenomena must be detected to determine whether a process should be terminated to ensure a wear's safety. For example, spasm is classified as the instant type or the sustaining type. For a sustaining spasm, the training process must be halted by turning off the exoskeleton system. But the instant type of spasm vanishes soon after it happens, and the exercising process may be allowed to continue without causing harm.

In the experiments, the gait rehabilitation was performed, and the instant spasm and tremor were assumed to happen during the test process. The spasm and tremor can be induced intentionally and spontaneously by a healthy subject in the test. They were intended to vanish soon after they happened. Figures 11–16 display the trajectories of the hip joint using the proposed LADRC, LESO-based SMC, and LESO-based FTSMC at the walking speeds of 0.15 m/s and 0.225 m/s. From the results, even though the instant spasm and tremor temporarily led to larger tracking errors, the rehabilitation process still continued with stable rehabilitation trajectory tracking for the three controllers after these phenomena quickly disappeared. However, the comparisons showed that the tracking performance for the LESO-based FTSMC was superior to the other two due to its better robustness to external disturbances. Moreover, the fast walking speed resulted in severe tracking errors for a brief moment when encountering these phenomena, owing to the response frequency.

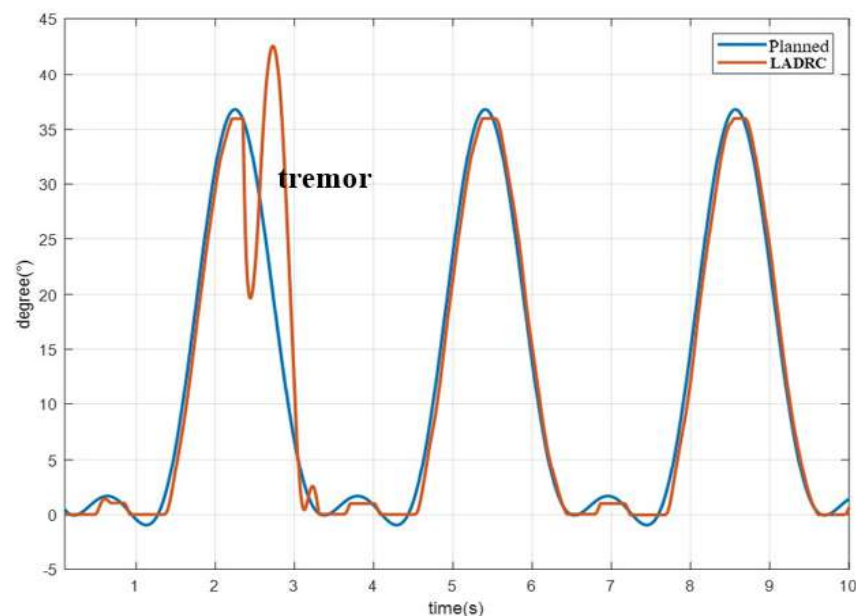


Figure 11. Trajectories of hip joint by LADRC with spasm and tremor occurring at walking speed = 0.15 m/s.

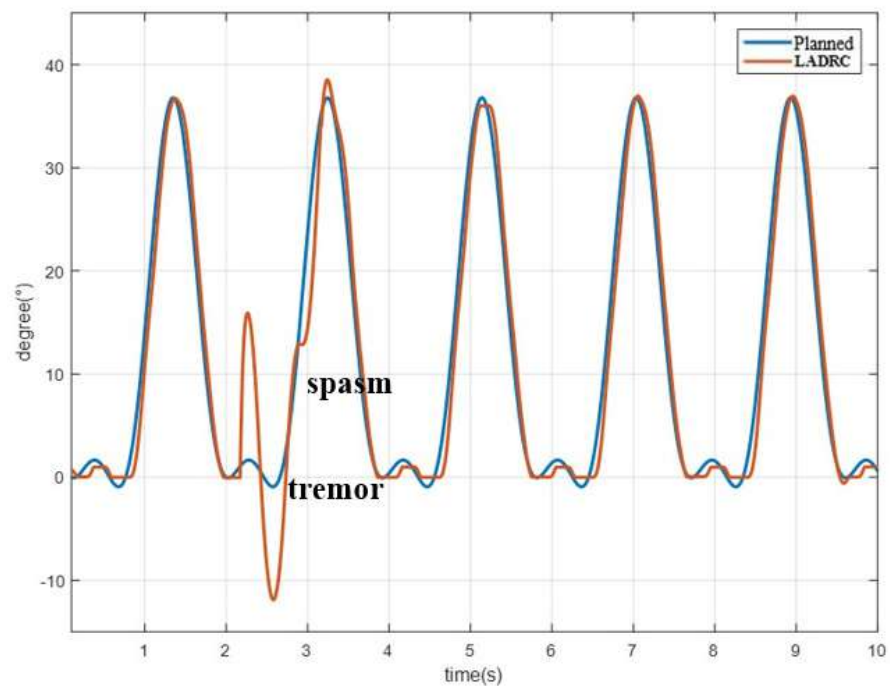


Figure 12. Trajectories of hip joint by LADRC with spasm and tremor occurring at walking speed = 0.225 m/s.

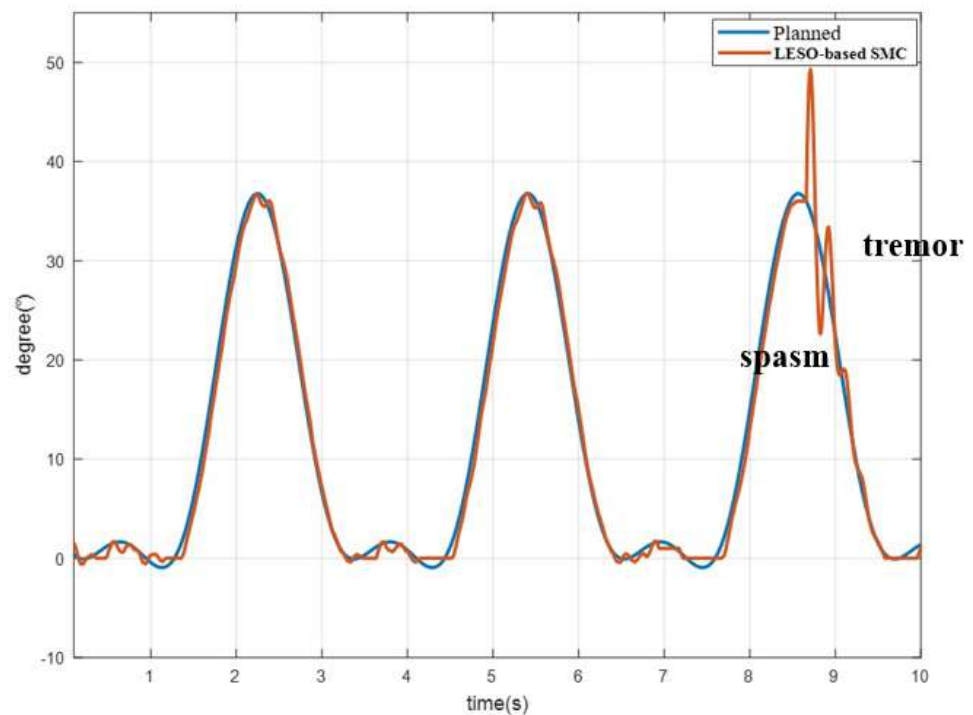


Figure 13. Trajectories of hip joint by LESO-based SMC with spasm and tremor occurring at walking speed = 0.15 m/s.

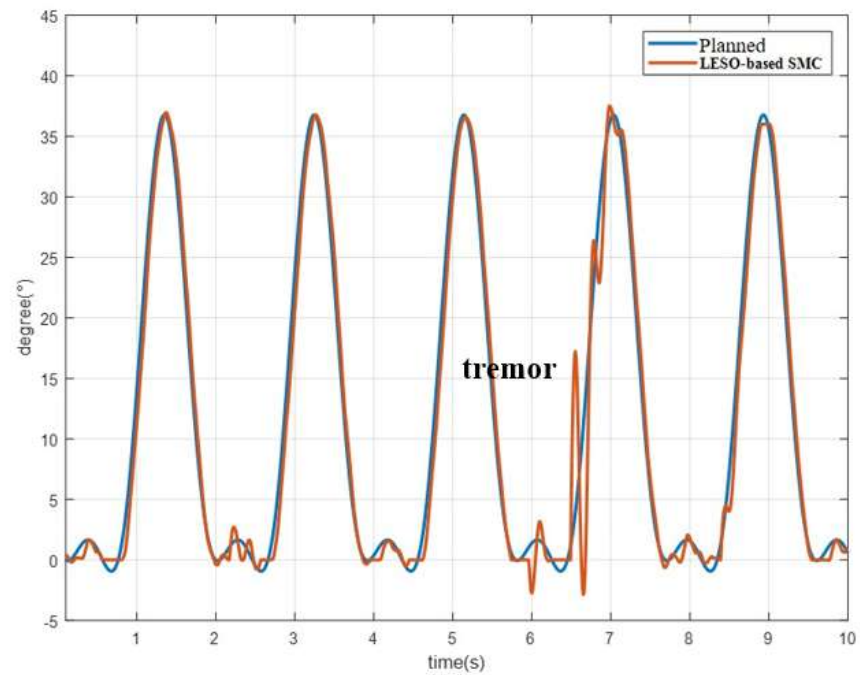


Figure 14. Trajectories of hip joint by LESO-based SMC with spasm and tremor occurring at walking speed = 0.225 m/s.

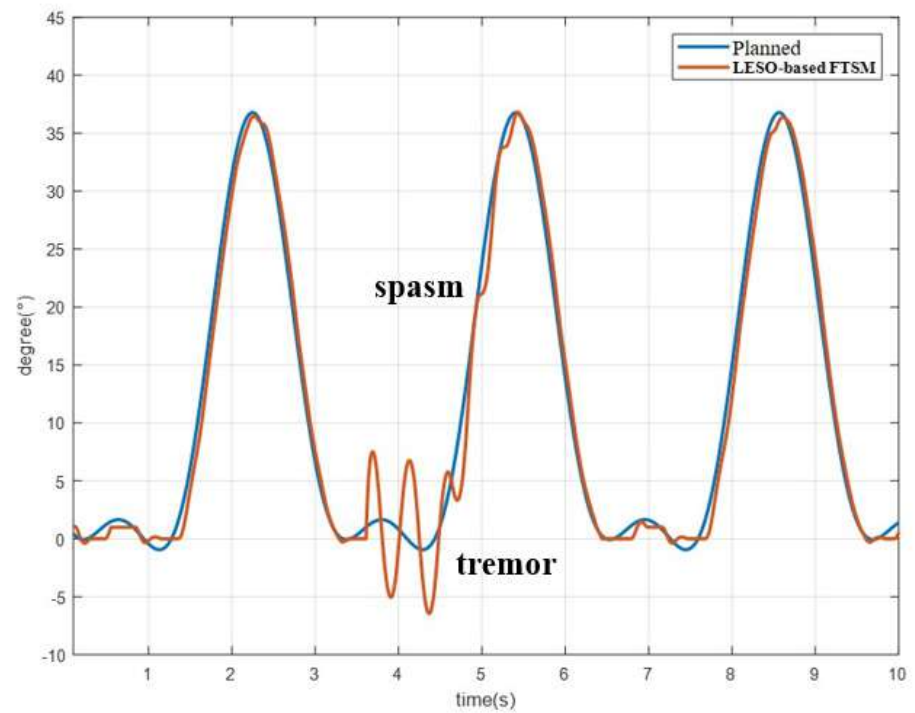


Figure 15. Trajectories of hip joint by LESO-based FTSM with spasm and tremor occurring at walking speed = 0.15 m/s.

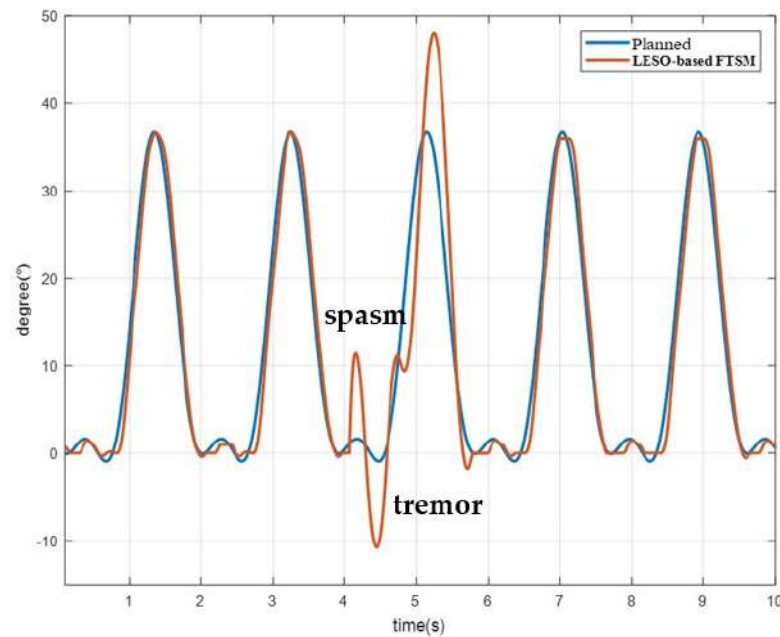


Figure 16. Trajectories of hip joint by LESO-based FTSM with spasm and tremor occurring at walking speed = 0.225 m/s.

4.3. Rehabilitation Experiment on Ascending

In the tests, a subject wore the robotic hip exoskeleton to ascend a staircase for gait rehabilitation, as shown in Figure 17. Each stair was 18 cm in height, and the ascending speed was specified as 4 steps per 10 secs, but with a difference of one step per stride and two steps per stride, which implies that the gait had a faster walking speed for one step per stride. Only the LESO-based FTSMC were used for the ascending gait rehabilitation owing to the superior tracking performance. Figures 18 and 19 describe the trajectories of the hip joint for ascending by one step and two steps per stride, respectively. The ascending results show that the tracking performance of one step per stride was inferior to two steps per stride due to walking speed. Additionally, the larger tracking errors often happened at the stance phase when more steps per stride were taken.



Figure 17. Ascending experiment for gait rehabilitation with robotic hip exoskeleton.

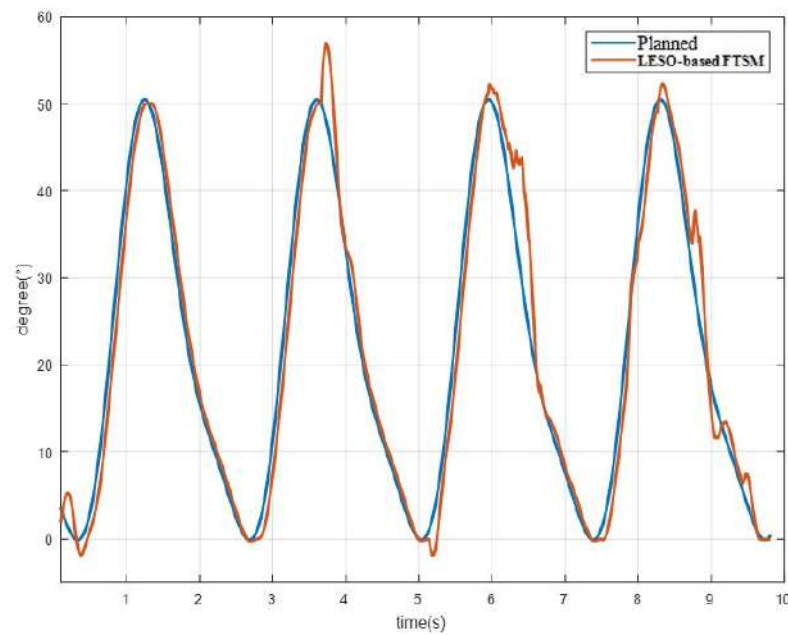


Figure 18. Trajectories of hip joint for ascending by one step per stride.

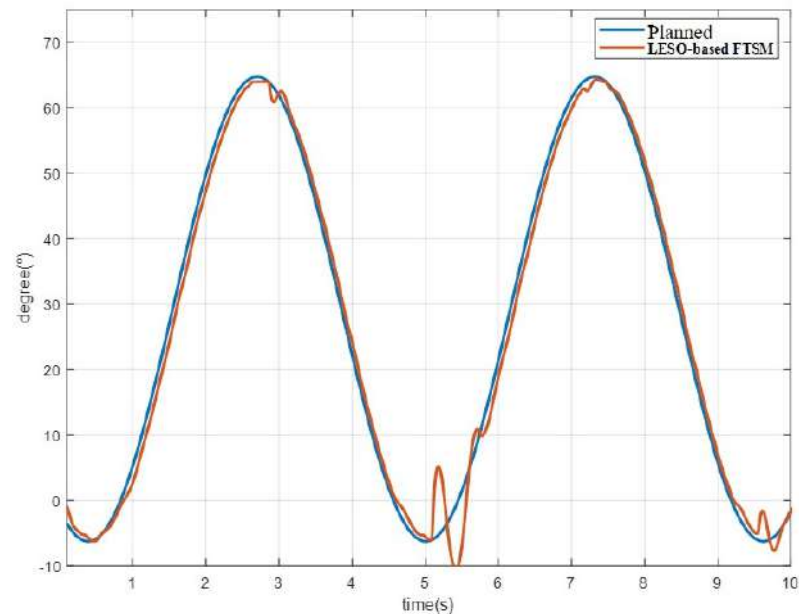
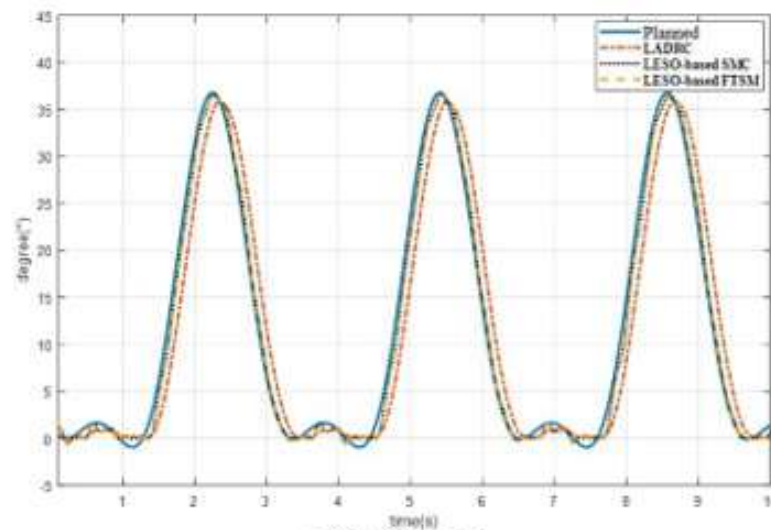


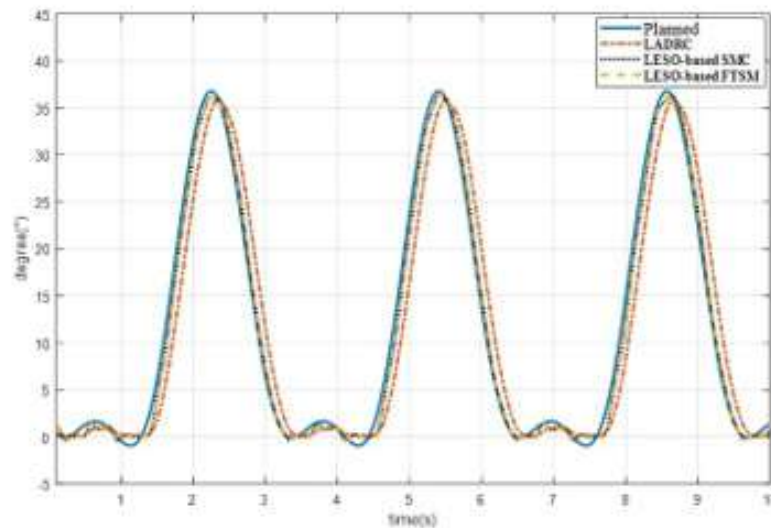
Figure 19. Trajectories of hip joint for ascending by two steps per stride.

4.4. Walking Experiments for Different Subjects

In this subsection, walking experiments were implemented for different subjects, in which two more subjects, namely subject B with 1.65 m height/57 kg weight and C with 1.81 m height/72 kg weight, were tested. The identical prerecorded gait trajectory at the walking speed of 0.15 m/s for the hip joints of the robotic hip exoskeleton was used for rehabilitation exercises. The slower walking speed was employed to ensure a stable gait. The following rehabilitation trajectory was controlled by the aforementioned three controllers. The trajectories of hip joints for the different subjects wearing the robotic hip exoskeleton are depicted in Figure 20. Even for different subjects with the distinctive heights and weights, the results show that the gait trajectories can be validated as a stable rehabilitation process under the proposed controls.



(a) Subject B.



(b) Subject C.

Figure 20. Trajectories of hip joint for different subjects.

The comparisons of hip joint trajectories for the subjects are presented in Table 2. For subject B, the RMSEs of trajectories by the proposed three controllers did not vary much more, and had smaller values as compared to subjects A and C. But for the subjects A and C with comparatively larger weights, the RMSEs of the rehabilitation trajectories could be decreased noticeably by LESO-based nonlinear controllers. The results showed that a heavy subject, implying larger inertia of the lower extremities, may result in a larger disturbance during walking. The linear LADRC was not enough to compensate the estimated disturbance errors. In addition, the wearer's height did not noticeably affect the trajectory tracking performance.

Table 2. RMSE of different subjects' hip joint trajectories for LADRC, LESO-based SMC, and LESO-based FTSMC.

Controller \ Subject	A	B	C
LADRC	3.685461°	0.654712°	3.688961°
LESO-based SMC	1.172696°	0.62858°	1.15422°
LESO-based FTSMC	1.145927°	0.627559°	1.141448

5. Evaluation of Rehabilitation Assistance

To evaluate the effects of the robotic hip exoskeleton on rehabilitation assistance, a three-dimensional motion captured system along with EMG sensors and force plates was used to measure the joint angles, bio-signal EMGs, and ground reaction forces.

In the motion-captured system, ten infrared cameras were deposited around a test field. Fifty-one reflectors were attached to the subject's body to mark for human model building. Force plates were put on the path along the subject's forward direction to measure the ground reaction forces. In addition, EMG sensors were also mounted to the skin to measure the muscle activation, in which four wireless EMG sensors were respectively pasted to the vastus lateralis, rectus femoris, gluteus medius, and biceps femoris of the thigh. As shown in Figure 21, a subject wore the robotic hip exoskeleton to execute a power assistance test for gait rehabilitation, the infrared cameras around the test field captured the images of reflectors, and then the human model could be rebuilt in a skeleton frame using the software ViconNexus2.8. The testing process based on the LESO-based FTSMC for the power assistance of gait rehabilitation is presented in Figure 22.



Figure 21. A subject wore the robotic exoskeleton with EMG sensors and reflectors attached to his body.



Figure 22. Testing process for power assistance of gait rehabilitation.

Figure 23 presents the ground reaction forces at walking with and without a robotic hip exoskeleton. The results showed that the ground reaction forces for both test cases had no apparent variations.

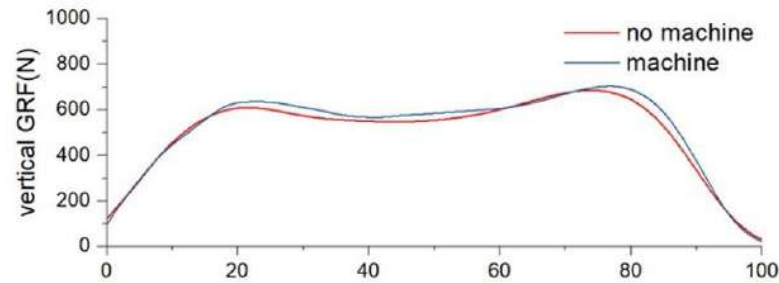


Figure 23. Ground reaction forces at walking.

The flexion/extension motion of the human's thigh is mainly controlled by the gluteus medius; therefore, only the EMG signals of the gluteus medius are displayed in Figure 24, in which the smaller peak value of the blue line implies an effective power assistance as one wears the robotic hip exoskeleton to execute a gait rehabilitation exercise.

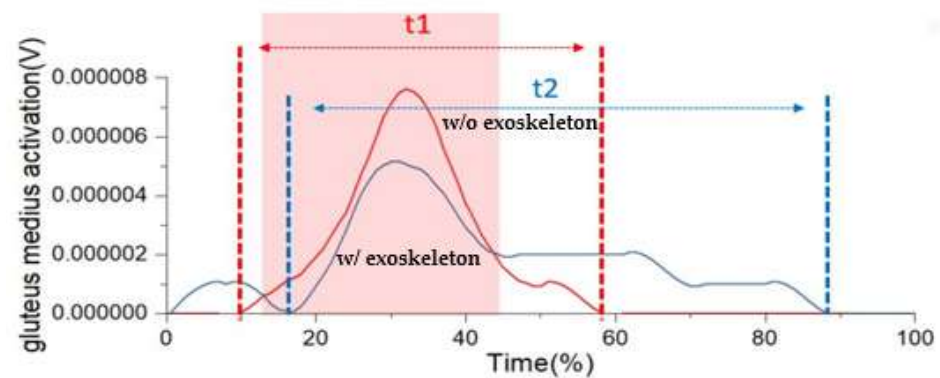


Figure 24. EMG signals of gluteus medius while walking.

6. Discussion of the Robotic Hip Exoskeleton for Rehabilitation

Based on the obtained results, the developed robotic hip exoskeleton can very much assist gait rehabilitation. For the experiments on walking, faster walking speeds make a disturbance more significant, and thus poor tracking performance is obtained by the LADRC due to its linear controller with constant gains. Moreover, in the LADRC, the estimated hip joint angles, instead of the measured angles, are fed back to synthesize the control signals. As such, the tracking performance is worse with the estimated tracking errors. However, the tracking performance can be improved by the proposed LESO-based FTSMC because the controller can approach a designated error plane rapidly and dynamically. In addition, walking should be limited to a slower speed for better tracking performance and safety.

While executing walking exercises using the robotic hip exoskeleton, some manifestations may occur and become disturbances to the designated gait trajectory. The results demonstrate that the proposed controllers can stabilize the ensuing rehabilitation process after the instant spasms and tremors vanish. However, if violent disturbances last continuously during gait rehabilitation, tracking errors cannot not be compensated by the LESO-based FTSMC. Thus, the exoskeleton system cannot be applied to all situations, for instance the sustaining type of spasm. In future clinical usage, these phenomena must be detected and monitored using appropriate sensors to determine whether a rehabilitation process should be terminated right away to ensure the wearer's safety. Furthermore, these physical phenomena accompanied with a faster gait rehabilitation may often lead to a

walking imbalances and result in unpredicted damage to users. Therefore, balance recovery may be an important research topic for lower-limbed exoskeletons.

When a human ascends steps, more metabolic energy and balance are required. In the ascending experiments in Section 4.3, the designed LESO-based FTSMC can stabilize the ascending trajectory effectively. Based on the comparisons of tracking performance, a slower gait with one step per stride by the robotic hip exoskeleton is better to achieve a stable ascending rehabilitation. If more steps per stride in the gait are taken to implement an ascent, a shaking gait trajectory is generated at the single supported stage. The resulting tracking errors may be solved by torso regulation of the robotic exoskeletons such that stabilization can be guaranteed on ascending.

Trajectory tracking performance was investigated for more subjects with different heights and weights. Based on Table 2, the tracking performance is not noticeably related to a subject's height, which is relevant to leg length. However, the inertia of the lower extremity proportional to weight gives rise to an un-modeled disturbance that leads to poor tracking performance, which means that the inertia of a leg plays an important role in the performance of gait rehabilitation. Although the proposed LESO-based nonlinear controllers can make an improvement in gait performance for heavy users, it also gives a suggestion that the user-defined control gain b_0 in Equation (2) should be dynamically tuned according to the user's weight.

Finally, from the evaluation of the effects of the robotic hip exoskeleton for rehabilitation assistance in Section 5, the results of ground reactions reveal that the proposed robotic hip exoskeleton can truly carry out a normal gait using the LESO-based FTSMC. Moreover, the gluteus medius controls the flexion/extension motion of a leg and affects the stability of hip joints, and smaller gluteus medius activation demonstrate that the robotic hip exoskeleton can provide assistance for walking stabilization.

7. Conclusions

This paper concludes with the following main contributions: a 4-DOF robotic hip exoskeleton was proposed to perform a gait rehabilitation exercise smoothly and robustly. Research efforts were also concentrated on the controller design for the reliable implementation of the walking assistance. Because every user has different dynamic parameters, the model-free LADRC, LESO-based SMC, and LESO-based FTSMC were developed for the robotic hip exoskeleton to effectively implement the gait rehabilitation.

The tracking error analyses conducted by the gait rehabilitation experiments on walking and ascending validated the capability of the robotic hip exoskeleton. Moreover, the performance comparisons demonstrate the superiority of the LESO-based FTSMC to the other two controllers. More noticeably, the executed gait rehabilitation maneuvers also validate the capability and robustness of the designed robotic hip exoskeleton when instant spasms and tremors happen. Additionally, the disturbance resulting from a subject's weight can be compensated well by the LESO-based FTSMC.

Finally, the evaluation of power assistance provided validation for the effective power assistance as one wears the robotic hip exoskeleton to execute walking. In the future, it is expected that a potential device for gait rehabilitation will be provided to patients suffering from muscle weakness through the help of clinical trials.

Author Contributions: Conceptualization: H.-J.L.; C.-T.C.; Investigation: S.-H.H.; C.C.; H.-J.L.; Methodology: S.-H.H.; C.C.; H.-J.L.; C.-T.C.; Software: S.-H.H.; C.C.; Supervision: C.-T.C.; Validation: S.-H.H.; C.-T.C.; Writing—original draft: S.-H.H.; C.C.; C.-T.C.; Writing—review & editing: S.-H.H.; C.-T.C. All authors have read and agreed to the published version of the manuscript.

Funding: This research was supported by the Ministry of Science and Technology of Taiwan under the Grant Nos. MOST 108-2321-B-027-001 and MOST 108-2221-E-003-024-MY3.

Institutional Review Board Statement: The ethics application number N201903077 was issued by TMU-Joint Institutional Review Board on 2019/06/15.

Informed Consent Statement: Not applicable.

Data Availability Statement: The data that support the findings of this research are available from the corresponding author, [C.T. Chen], upon reasonable request.

Conflicts of Interest: The authors declare no conflict of interest.

References

1. Burgar, C.G.; Lum, P.S.; Shor, P.C.; Van der Loos, H.F.M. Development of robots for rehabilitation therapy: The Palo Alto VA/Stanford experience. *J. Rehabil. Res. Dev.* **2000**, *37*, 663–673.
2. Bogue, R. Exoskeletons and robotic prosthetics: A review of recent developments. *Ind. Robot. Int. J.* **2009**, *36*, 421–427. [[CrossRef](#)]
3. Kong, K.; Jeon, D. Design and control of an exoskeleton for the elderly and patients. *IEEE/ASME Trans. Mechatron.* **2006**, *11*, 428–432. [[CrossRef](#)]
4. Xiao, F.; Gao, Y.; Wang, Y.; Zhu, Y.; Zhao, J. Design and evaluation of a 7-DOF cable-driven upper limb exoskeleton. *J. Mech. Sci. Technol.* **2018**, *32*, 855–864. [[CrossRef](#)]
5. Nycz, C.J.; Bützer, T.; Lambercy, O.; Arata, J.; Fischer, G.S.; Gassert, R. Design and characterization of a lightweight and fully portable remote actuation system for use with a hand exoskeleton. *IEEE Robot. Autom. Lett.* **2016**, *1*, 976–983. [[CrossRef](#)]
6. Zoss, A.B.; Kazerooni, H.; Chu, A. Biomechanical design of the Berkeley lower extremity exoskeleton (BLEEX). *IEEE/ASME Trans. Mechatron.* **2006**, *11*, 128–138. [[CrossRef](#)]
7. Ortlieb, A.; Bouri, M.; Baud, R.; Bleuler, H. An assistive lower limb exoskeleton for people with neurological gait disorders. In Proceedings of the 2017 International Conference on Rehabilitation Robotics (ICORR), London, UK, 17–20 July 2017; pp. 441–446.
8. Wu, Q.; Wang, X.; Du, F.; Zhang, X. Design and control of a powered hip exoskeleton for walking assistance. *Int. J. Adv. Robot. Syst.* **2015**, *12*, 18. [[CrossRef](#)]
9. Hyun, D.J.; Park, H.; Ha, T.; Park, S.; Jung, K. Biomechanical design of an agile, electricity-powered lower-limb exoskeleton for weight-bearing assistance. *Robot. Auton. Syst.* **2017**, *95*, 181–195. [[CrossRef](#)]
10. Sankai, Y. Hal: Hybrid Assistive Limb Based on Cybernetics. In *Robotics Research*; Springer: Berlin/Heidelberg, Germany, 2010; pp. 25–34.
11. Yana, T.; Cempinia, M.; Oddoa, C.M.; Vitiello, N. Review of assistive strategies in powered lower-limb orthoses and exoskeletons. *Robot. Auton. Syst.* **2015**, *64*, 120–136. [[CrossRef](#)]
12. Chen, B.; Zi, B.; Qin, L.; Pan, Q. State-of-the-art research in robotic hip exoskeletons: A general review. *J. Orthop. Transl.* **2020**, *20*, 4–13. [[CrossRef](#)]
13. Anama, K.; Al-Jumaily, A.A. Active exoskeleton control systems: State of the art. *Procedia Eng.* **2012**, *41*, 988–994. [[CrossRef](#)]
14. Seo, K.; Lee, J.; Park, Y.J. Autonomous hip exoskeleton saves metabolic cost of walking uphill. In Proceedings of the 2017 International Conference on Rehabilitation Robotics (ICORR), London, UK, 17–20 July 2017; pp. 246–251.
15. Giovacchini, F.; Vannetti, F.; Fantozzi, M.; Cempini, M.; Cortese, M.; Parri, A. A lightweight active orthosis for hip movement assistance. *Robot. Auton. Syst.* **2015**, *73*, 123–134. [[CrossRef](#)]
16. Nagarajan, U.; Aguirre-Ollinger, G.; Goswami, A. Integral admittance shaping: A unified framework for active exoskeleton control. *Robot. Auton. Syst.* **2016**, *75*, 310–324. [[CrossRef](#)]
17. Zhang, T.; Tran, M.; Huang, H. Design and experimental verification of hip exoskeleton with balance capacities for walking assistance. *IEEE/ASME Trans. Mechatron.* **2018**, *23*, 274–285. [[CrossRef](#)]
18. Teramae, T.; Noda, T.; Morimoto, J. EMG-based model predictive control for physical human—Robot interaction: Application for assist-as-needed control. *IEEE Robot. Autom. Lett.* **2018**, *3*, 210–217. [[CrossRef](#)]
19. Hsu, S.H.; Changcheng, C.; Chen, C.-T.; Wu, Y.-C.; Lian, W.-Y.; Li, T.-M.; Huang, C.-E. Design and evaluation of a wearable lower limb robotic exoskeleton for power assistance. In Proceedings of the 2020 IEEE International Conference on Systems, Man, and Cybernetics (SMC), Toronto, ON, Canada, 11–14 October 2020; pp. 2465–2470.
20. Long, Y.; Du, Z.; Cong, L.; Wang, W.; Zhang, Z.; Dong, W. Active disturbance rejection control based human gait tracking for lower extremity rehabilitation exoskeleton. *ISA Trans.* **2017**, *67*, 389–397. [[CrossRef](#)] [[PubMed](#)]
21. Gao, Z. Scaling and bandwidth-parameterization based controller tuning. In Proceedings of the 2006 American control conference, Minneapolis, MN, USA, 14–16 June 2006; pp. 4989–4996.
22. Han, J. From PID to active disturbance rejection control. *IEEE Trans. Ind. Electron.* **2009**, *56*, 900–906. [[CrossRef](#)]
23. Chen, C.; Gao, H.; Ding, L.; Li, W.; Yu, H.; Deng, Z. Trajectory tracking control of WMRs with lateral and longitudinal slippage based on active disturbance rejection control. *Robot. Auton. Syst.* **2018**, *107*, 236–245. [[CrossRef](#)]
24. Xia, Y.; Zhu, Z.; Fu, M.; Wang, S. Attitude tracking of rigid spacecraft with bounded disturbances. *IEEE Trans. Ind. Electron.* **2010**, *58*, 647–659. [[CrossRef](#)]
25. Yu, X.; Zhihong, M. Fast terminal sliding-mode control design for nonlinear dynamical systems. *IEEE Trans. Circuits Syst. I Fundam. Theory Appl.* **2002**, *49*, 261–264.
26. McDonald, C.M. Limb contractures in progressive neuromuscular disease and the role of stretching, orthotics, and surgery. *Phys. Med. Rehabil. Clin. N. Am.* **1998**, *9*, 187–211. [[CrossRef](#)]